Journal of Membrane Science and Research 7 (2021) 152-165

Journal of Membrane Science & Research

journal homepage: www.msrjournal.com

Research Paper

Adsorption of Cadmium (II) Ions from Aqueous Solutions using Poly(Amidoamine)/ Multi-Walled Carbon Nanotubes Doped Poly(Vinylidene Fluoride-Co-Hexafluoropropene) Composite Membrane

Lutendo Evelyn Macevele [1], Kgabo Lydia Maureen Moganedi [2], Takalani Magadzu [1,*]

[1] *Department of Chemistry, University of Limpopo, Private Bag x1106, Sovenga 0727, South Africa*
[2] *Department of Biochemistry, Microbiology and Biotechnology, University of Limpopo, Private Bag x1106, Sovenga 0727, South Africa*

Article info

Received 2020-03-01
Revised 2020-06-19
Accepted 2020-07-15
Available online 2020-07-15

Keywords

PVDF-HFP
Composite membrane
Multi-walled carbon nanotubes
Poly-amidoamine
Cd(II) ions
Adsorption capacity

Highlights

- Thermally stable, hydrophilic composite membranes with high surface area
- 1 wt.% PAMAM-MWCNTs/PVDF-HFP showed maximum adsorption ability of 167 mg/g at 25°C
- Cd(II) adsorption conformed to Freundlich model
- Adsorption remained above 90% after four reusability cycles

Graphical abstract

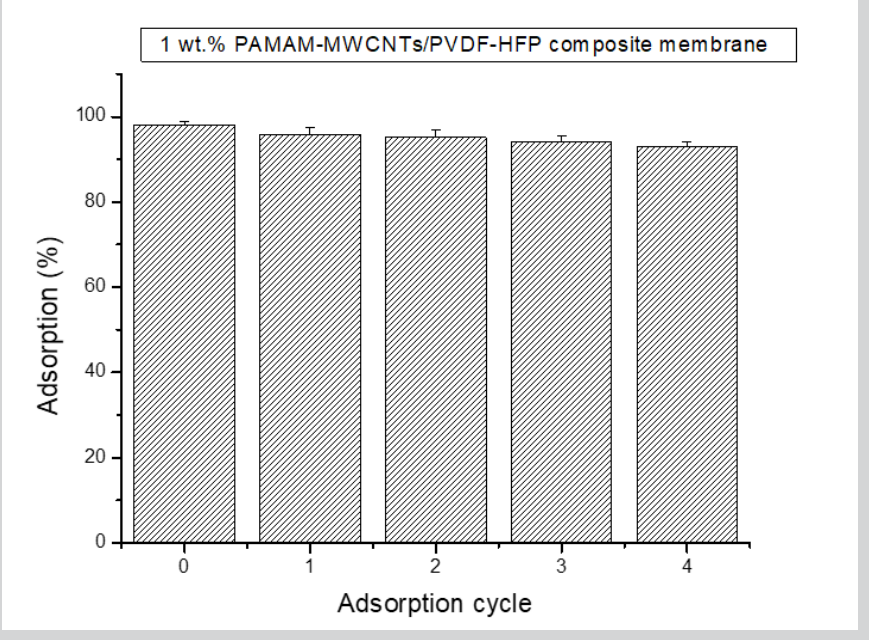

Abstract

Composite membranes consisting of Poly(vinylidene fluoride-co-hexafluoropropene) (PVDF-HFP) blended with functionalised multi-walled carbon nanotubes (MWCNTs) and poly-amidoamine (PAMAM) were prepared using a phase inversion technique for adsorptive elimination of Cd (II) ions from contaminated water samples. Upon the addition of PAMAM-MWCNTs on PVDF-HFP, a stable, microporous structure with enhanced surface area and hydrophilic composite membranes were obtained; as confirmed by Focused Ion Beam Scanning Electron Microscopy (FIB-SEM), Fourier transform infrared (FTIR), Thermogravimetric analysis (TGA), Brunauer-Emmett-Teller (BET) analysis and contact angle measurements. The pH, adsorption isotherm, thermodynamic parameters and reusability of the composite membranes were investigated in batch experiments. The maximum adsorption capacity of 1 wt.% PAMAM-MWCNTs/PVDF-HFP composite membrane calculated by Langmuir model was 167 mg/g at 25°C and pH 6.5. All composite membranes demonstrated that the Cd(II) ions adsorption conformed to Freundlich model (R^2 = 0.999), which suggests that the adsorption process is multilayer. In addition, the thermodynamic parameters indicated that the adsorption process is spontaneous and endothermic in nature. The adsorption capacity of 1 wt.% PAMAM-MWCNTs/PVDF-HFP composite membrane remained above 90% after four reusability cycles, as confirmed by Inductively coupled plasma-optical emission spectrometry (ICP-OES) analysis. The 1 wt.% PAMAM-MWCNTs/ PVDF-HFP composite membrane exhibited higher selectivity coefficients towards Cd(II) in Cu(II), Zn(II) and Ni(II) binary metal solutions.

1. Introduction

Water pollution by heavy metals is one of the main environmental concerns throughout the world, due to their recalcitrant and persistence [1,2]. Heavy metal contamination occurs in aqueous waste streams in many industries, such as surface finishing industry, energy and fuel production, fertilizer and pesticide industry, metallurgy, etc. [1]. Heavy metals associated with these activities among others includes cadmium, lead and arsenic that

* Corresponding author:E-mail address: Takalani.Magadzu@ul.ac.za (T. Magadzu)
DOI: 10.22079/JMSR.2020.121858.1351

often pose challenges especially in developing countries [3,4]. These heavy metals are not biodegradable, and tend to accumulate in living organisms, causing various diseases including cancer [5]. Metal toxicity depends upon the absorbed dosage, the route of exposure and duration of exposure, i.e. acute or chronic [6].

Heavy metals such as cadmium is known to be highly toxic and has been reported to cause kidney and liver damage, hypertension, lung insufficiency, bone lesions, cancer, etc. [7–9]. Cadmium (Cd) poisoning has been reported from many parts of the world, and its levels can be measured in the blood, urine, hair, nail and saliva samples. Patients with cadmium toxicity need gastrointestinal tract irrigation, supportive care, chemical decontamination and any other suitable alternative treatment [8]. The permissible limits of cadmium in drinking water recommended by the World Health Organization (WHO) and the South African National Standard (SANS 241) is ≤ 3 µg/L [10,11], hence the removal of Cd(II) ions from potable and wastewater is crucial.

A variety of methods used to remove heavy metals include; chemical precipitation, electroplating, ion-exchange, membrane processes, evaporation, etc. [1,12,13]. However, most of these processes have numerous drawbacks such as unpredictable metal ion removal, high reagent requirements and generation of toxic sludge [13]. Adsorption is among the most successful methods, because it is often reversible, easy to implement, less costly, and highly efficient for advanced wastewater treatment of industrial effluent containing metals [13–16].

Carbon nanomaterials such as carbon nanotubes (CNT), chitosan, graphene, and other functional materials have shown promising adsorption capacities towards the removal of metal ions and dyes, as compared to traditional methods; this is due to their high surface area, chemical and mechanical properties [14]. For example, a study by Tohdee et al. [17] revealed that a cationic modified bentonite showed improved adsorption capacities, q_{max} of 50.76 and 35.21 mg/g for both Cu(II) and Zn(II), respectively [17]. Other improvements in adsorptions capacities were reported on graphene oxide-wrapped magnetite nanoclusters [18] and functionalised CNTs [19].

Very few studies have investigated the interaction of composite membranes with heavy metals, even though such composites have shown promising adsorption capacities. For example, zirconium-poly(vinyl alcohol) modified Polyvinylidene fluoride (PVDF) membrane have shown the maximum adsorption capacity for phosphate and lead of 74 and 121 mg/g, respectively [20,21]. Nthumbi et al. [22] has also shown adsorption of trace elements from water using functionalised PVDF/PAN composite that had an adsorption efficiency for Pb(II) and Cd(II) ions of 90 and 80%, respectively.

Polymeric materials such as poly(amidoamine) (PAMAM) dendrimers enhances the heavy metal adsorption capacity of CNT, due to the abundance of amino groups [23]. To the best of our knowledge no reports on the use of PAMAM combined with PVDF-HFP as composite material for heavy metal adsorption has been conducted thus far. The PVDF-HFP polymeric material possesses high dielectric constant, good mechanical properties [24], as well as high porosity, hydrophilicity and fouling resistance as reported previously [25]. Hence, the study has evaluated the effects of PAMAM modified MWCNTs on adsorption properties of PVDF-HFP membranes (i.e. 1 wt.% PAMAM-MWCNTs/PVDF-HFP composite membranes prepared by phase inversion). The batch experiments for Cd(II) ions adsorption were carried out and the effects of different operational parameters such as pH, kinetics, adsorption isotherm, reusability and competitive adsorption were investigated.

2. Materials and method

2.1. Materials

All chemicals were of analytical reagent grade and were used as received, whilst some were further purified when required. Poly(vinylidene fluoride-co-hexafluoropropene), N,N-dimethylacetamide, nitric acid, sulphuric acid, MWCNTs, polyethylene glycol, polyvinylpyrrolidone, ethylenediamine, methyl acrylate, toluene 2,4-diisocyanate, methanol and ethanol were all purchased from Sigma Aldrich, Darmstadt, Germany.

2.2. Preparation of MWCNTs functionalised with the NCO group

About 2 g of MWCNTs-COOH (MWCNTs functionalised using 1:3 HNO_3/H_2SO_4) were dispersed in anhydrous acetone (20 mL) while stirring for 30 minutes [26]. This was followed by drop-wise addition of 4 mL of toluene 2,4-diisocyanate, under dry nitrogen atmosphere at 25 °C for 1 h, to form a multi-walled carbon nanotubes functionalised with isocyanate groups (MWCNTs-NCO). The mixture was allowed to stir for an additional 23 h. After 24 h, the MWCNTs-NCO was washed with anhydrous acetone to completely remove the residuals, filtered and left to dry at room temperature overnight [27].

2.3. Preparation of MWCNTs-NH_2 initiator from MWCNTs-NCO

MWCNTs-NCO was reacted with an excess of ethylene diamine to obtain MWCNTs containing amino groups (MWCNTs-NH_2) as follows: Approximately 0.3 g of MWCNTs-NCO synthesised was dispersed in 20 mL of anhydrous acetone under sonication for 30 minutes, and then an excess amount of ethylenediamine (EDA) was added drop-wise under stirring for 1 h at 25 °C under a nitrogen atmosphere. The reaction was allowed to continue for 24 h. The resulting solid was washed with anhydrous methanol, filtered and dried overnight under vacuum, generating MWCNTs-NH_2 [28].

2.4. Preparation of poly(amidoamine) dendrimer/multi-walled carbon nanotubes (PAMAM-MWCNTs) initiated by MWCNTs-NH_2

Michael addition of methyl acrylate (MA) to peripheral amino groups was carried out following a procedure described by Yuan et al. [29]: Briefly, approximately 0.1 g of MWCNTs-NH_2 was dispersed in methanol (20 mL) under stirring and then added to 40 mL of methanol/MA solution (1:1). The mixture was allowed to react for 48 h at 30 °C under nitrogen atmosphere. The resulting solid was filtered, washed with distilled water and dried; yielding functionalised MWCNTs containing the "first generation" ester group (MWCNTs-$G_{0.5}$-$COOCH_3$).

The amidation of the terminal groups of MWCNTs-$COOCH_3$ was carried out by the same procedure as discussed above using ethylene diamine (EDA) instead of MA: A certain amount of MWCNTs-$G_{0.5}$-$COOCH_3$ was dispersed in methanol (20 mL) under stirring and then added to 40 mL of methanol/EDA solution (1:1). The mixture was allowed to react for 48 h at 30 °C. The resulting solid was washed with methanol, filtered, and dried; yielding functionalised MWCNTs containing the "first generation" amino groups (MWNTs-G_1-NH_2) which is PAMAM-MWCNTs.

2.5. Preparation of 1 wt.% MWCNTs/PVDF-HFP and 1 wt.% PAMAM-MWCNTs/PVDF-HFP composite membranes

PVDF-HFP polymeric membranes were prepared by a phase inversion process as described previously [25], with modification. Approximately 2.0 g of PVDF-HFP polymer was dissolved in 15 mL of N,N-Dimethylacetamide (DMAc) at 80°C to form a polymer solution. To this solution, about 0.62 g of PVP was added (to enhance pore formation) and the reaction mixture was stirred for 2 h at 80°C. Separately, 0.021 g of functionalised MWCNTs were sonicated in 5 mL of DMAc for 30 min. The final mixture was prepared by adding functionalised MWCNTs to a solution of PVDF-HFP. The mixture was allowed to stir for an additional 1 h and then hand cast into a glass plate using a casting knife (Elcometer 3580 adjustable bird film applicator, BAMR, Cape Town, South Africa) of 180 µm thickness. The prepared membranes were first dried in a vacuum oven at 80°C (for 30 s) for solvent pre-evaporation and then coagulated using distilled water (at 5°C) as the anti-solvent. After complete coagulation, the membranes were dried on plain sheets of paper at room temperature. A similar procedure was followed to prepare 1 wt.% PAMAM-MWCNTs/PVDF-HFP composite membranes. For preparation of 1 wt.% PAMAM-MWCNTs/PVDF-HFP composite membrane, sonicated PAMAM-MWCNTs (0.021 g in 5 mL DMAC) were added in the PVDF-HFP polymer solution.

2.6. Characterisation techniques

The surface functional groups were characterised by a Fourier transform infrared spectroscopy (Agilent Cary 600 series FTIR spectrophotometer) within the wavelength of 650 to 4000 cm^{-1}. The crystal phase of the membranes was analysed by a Philips X-Ray Diffractometer PW 1830 (XRD) at the 2θ range of 10 to 80° with Cu Kα (λ = 0.15405 nm). Thermogravimetric studies were carried out by TGA Q500 with a heating rate of 10°C min^{-1} under a nitrogen flow (40 ml min^{-1}) to measure the change in mass of membrane samples over a range of temperatures. The surface morphology and cross sections of the membranes was investigated by a Focused Ion Beam Scanning electron microscopy (FIB-SEM) (Auriga Zeiss SEM with Germini FESEM column), equipped with energy dispersal X-ray spectroscopy (EDX). Surface areas analyses were carried out using Micromeritics ASAP 2020 Brunauer–Emmett–Teller (BET) instrument.

2.7. Batch adsorption studies

The effect of pH on the adsorption capacity was examined by varying the initial pH of the solution. Approximately, 50 mL of cadmium (II) ions

standard solution (100 ppm) at different pH (4, 5, 5.5, 6, 6.5, 7 and 8) were prepared in glass vials and the membrane dosage of 0.5 g/L (i.e. 10 mg mass of the sample/20 mL volume of the solution) was added. About 0.1 M nitric acid (HNO_3) and 0.1 M sodium hydroxide (NaOH) were both used to adjust the pH of Cd(II) solutions. The Erlenmeyer flaks containing the metal solutions and the membranes were placed on a rotary shaker and agitated at room temperature (25 °C) for 48 hrs. At the end of 48 h, the residual Cd(II) concentration was analysed using the Atomic Absorption Spectrophotometer (AAS). The amount of metal ions adsorbed in milligram per gram and percentage removal of Cd(II) ions were determined using the mass balance equation 1 and 2, respectively [17,19]:

$$q_e = \frac{(C_o - C_e)V}{m} \tag{1}$$

$$\%removal = \frac{(C_o - C_e}{C_o} \times 100 \tag{2}$$

where q_e is the equilibrium adsorption amount (mg/g), C_o is the initial concentration of metals in solution (mg/L), C_e is the equilibrium concentration of the metal adsorbed in solution (mg/L), m is the mass of adsorbent (g), and V is the volume of solution (L) [17].

Adsorption studies were carried out by batch process. In batch process, PVDF-HFP based composite membranes (10 mg) were placed in Erlenmeyer flasks containing Cd(II) solutions (20 mL) with different initial concentrations (20-100 mg/L). The membrane dosage was 0.5 g/L and the pHs of the aqueous solutions were adjusted to 6.5 by 0.1 M nitric acid or 0.1 M sodium hydroxide solution. The Erlenmeyer flaks containing the metal solutions and the membranes were placed on a rotary shaker and agitated at different temperatures (15 °C, 25 °C, 35 °C and 45 °C) for 48 h. At the end of 48 h, the residual Cd(II) ions concentration was analysed using AAS. The same procedure was followed to study the effect of contact time from 0 to 1600 minutes. At predetermined times, the flasks were withdrawn from the shaker and the reaction mixtures were analysed using AAS.

In order to better understand the adsorption kinetics, the pseudo-first-order model (equation 3) and the pseudo-second-order model (equation 4), given as follows, were used [19,30]:

$$\ln(q_e - q_t) = \ln q_e - k_1 t \tag{3}$$

$$\frac{t}{q_t} = \frac{1}{k_2 q_e^2} + \frac{t}{q_e} \tag{4}$$

where q_e (mg/g) and q_t (mg/g) are the concentrations of Cd(II) adsorbed at equilibrium and at time t respectively. k_1 (min^{-1}) is the pseudo-first-order kinetic constant and k_2 (g/mg·min) is the pseudo-second-order rate constant of sorption.

The experimental data were fitted to both Langmuir and Freundlich isotherms, and the thermodynamic parameters were also evaluated. The Langmuir isotherm equation is expressed as shown in equation 5, and its linear form in equation 6 [31,32]:

$$q_e = \frac{q_{max} b C_e}{1 + bC_e} \tag{5}$$

$$\frac{1}{q_e} = \frac{1}{q_{max}} + \frac{1}{b q_{max} C_e} \tag{6}$$

where q_e is the equilibrium adsorption amount (mg/g), C_e (mg/L) is the equilibrium concentration of metal adsorbed in the solution, q_{max} (mg/g) represents the maximum adsorption capacity or the theoretical monolayer saturation capacity and b (L/mg) is the Langmuir equilibrium constant. The essential features of the Langmuir isotherm indicating the favourability of the adsorption (R_L, also called equilibrium parameter) is expressed by equation 7 [31,33]:

$$R_L = \frac{1}{1 + bC_o} \tag{7}$$

where C_o (mg/L) is the initial metal concentration and b is Langmuir equilibrium constant for adsorption (L/mg). The value of R_L indicates the type of Langmuir isotherm to either be unfavourable adsorption (R_L>1), linear (R_L = 1), favourable (0 < R_L < 1) or irreversible (R_L = 0).

The Freundlich model is expressed as shown in equations 8 and its linear equation expressed in equation 9 [31]:

$$q_e = K_f C_e^{1/n} \tag{8}$$

$$\ln q_e = \ln K_f + \frac{1}{n} \ln C_e \tag{9}$$

where q_e is the equilibrium adsorption amount (mg/g), C_e (mg/L) is the equilibrium concentration of metal adsorbed in the solution. K_f (mg/g) and n (dimensionless) are Freundlich constants which correspond to adsorption capacity and adsorption intensity, respectively.

Thermodynamic parameters were evaluated from the following equations [22]:

$$\Delta G^\circ = -RT \ln K_c \tag{10}$$

$$\ln K_o = \frac{\Delta S^\circ}{R} - \frac{\Delta H^\circ}{RT} \tag{11}$$

$$K_o = \frac{C_{ad}}{C_e} \tag{12}$$

where C_e (mg/L) is the equilibrium concentration of metal adsorbed in the solution and C_{ad} is the concentration of the metal in the adsorbent at equilibrium (mg/L). ΔG^o, ΔH^o and ΔS^o are changes in the standard Gibbs free energy (kJ/mol), standard enthalpy (kJ/mol) and standard entropy (J/mol/K). R is the gas constant (8.314 J/mol.K) and $\ln K_o$ is the rate constant and T is the temperature in Kelvin. The values of ΔH^o and ΔS^o are determined from the slope and the intercept from the plot of $\ln K_o$ versus 1/T.

Reusability studies of the three PVDF-HFP based composite membranes were performed by following the Cd(II) ions adsorption-desorption studies for four cycles. In order to study the reusability of the adsorbents, PVDF-HFP based composite membranes (0.5 g/L) were contacted with 20 mL of Cd(II) solution (100 ppm) for 48 h at 25°C. After 48 hours, the solutions were analysed and the final concentration of Cd(II) ions was determined using the AAS. The PVDF-HFP based composite membranes were recycled by immersing them separately into 50 mL of 0.5 M HNO_3 solutions for 1 h (for desorption to occur), and finally the adsorbents were washed thoroughly with distilled water and bicarbonate solution to remove HNO_3. The membranes were added again into another Cd(II) solution to start a new adsorption batch. The adsorption process was repeated 4 times to test the reusability of the adsorbents.

To evaluate the selectivity of the 1 wt.% PAMAM-MWCNTs/PVDF-HFP composite membrane, the following procedure was followed: An Erlenmeyer flask containing a mixture of Cd(II) solution (100 mg/L) and 1 wt.% PAMAM-MWCNTs/PVDF-HFP composite membranes (0.5 g/L) at a pH of 6.5, were placed on a rotary shaker for 48 h at 25 °C.

The distribution and selectivity coefficients of Cd(II) with respect to Cu(II), Ni(II) and Zn(II) can be obtained from the equilibrium binding data according to equation (13) and (14) [20]:

$$K_d = \frac{q_e}{C_e} \tag{13}$$

$$K = \frac{K_d[Cd(II)]}{K_d[X(II)]} \tag{14}$$

where K_d is the distribution coefficient (L/g), q_e is the amounts of metal ions adsorbed by the membrane (mg/g), C_e (mg/L) is the concentration of the metal at equilibrium, K is the selectivity coefficient and X represent the competing ions of Cu(II), Zn(II) and Ni(II).

3. Results and discussions

3.1 Characterisation of composites membranes

3.1.1. The FTIR profiles of MWCNTs, PAMAM-MWCNTs, PVDF-HFP, 1 wt.% MWCNTs/PVDF-HFP and 1 wt.% PAMAM-MWCNTs/PVDF-HFP nanocomposite membranes

Figure 1 (A and B) shows the FTIR profiles MWCNTs, PAMAM-MWCNTs, PVDF-HFP, 1 wt.% MWCNTs/PVDF-HFP and 1 wt.% PAMAM-MWCNTs/PVDF-HFP nanocomposite membranes. In Figure 1A (a), the peak intensities at 3210 and 1130 cm^{-1} can be attributed to the stretching vibrations of O-H and C-O stretching respectively. The peak intensity at 2295 cm^{-1} is attributed to C-H stretching mode suggesting that oxidation of the MWCNTs successfully introduced the carboxylic group (-COOH) on the walls of carbon nanotubes [34]. This peak at 2295 cm^{-1} slightly disappears in the presence of PAMAM, and the new peak at 2140 cm^{-1}, which is associated with asymmetric stretching of -NCO- groups slightly appears [27]. The absorption peak at 3210 cm^{-1} (Figure 1A (b)) is due to the stretching vibration of -NH- group and the bands peaking at 1620 and 1519 cm^{-1} correspond to amides (-CO-NH-) I and II, and this shows that PAMAM-MWCNTs dendrimers were favourably synthesised [23,35,36].

The peak intensities in Figure 1B for all the composite membranes between 1418 and 820 cm^{-1} (Figure 1B (a)) confirm the γ-phase crystalline structure of the PVDF-HFP polymer, which is present in all PVDF-HFP composites [27]. The peaks due to the O-H stretching mode of MWCNTs on 1 wt.% MWCNTs PVDF-HFP (Figure 1B(b)) was observed at 2980 cm^{-1}. The band at 3480 cm^{-1} appearing on 1 wt.% MWCNTs-PVDF-HFP is due to an O-H stretching mode of MWCNTs and this peak appears to be broader on 1 wt.% PAMAM-MWCNTs/PVDF-HFP as a result of PAMAM dendrimer attached to the -OH of the carboxylic groups on the walls of MWCNTs [34]. The peak at 1620 cm^{-1} (Figure 1B(c)) proves the existence of PAMAM-MWCNTs dendrimer on PVDF-HFP [35,36].

3.1.2. XRD profiles of PVDF-HFP, MWCNTs, 1 wt.% MWCNTs/PVDF-HFP, PAMAM-MWCNTs, and 1 wt.% PAMAM-MWCNTs/PVDF-HFP composite membranes

Figure 2 shows the XRD patterns of PVDF-HFP, MWCNTs, 1 wt.% MWCNTs/PVDF-HFP, PAMAM-MWCNTs and 1 wt.% PAMAM-MWCNTs/PVDF-HFP composite membranes. The noisy hump appearing at 2θ = 21° for PVDF-HFP membrane (Figure 2a) is ascribed to a graphitic structure of PVDF-HFP. The XRD profile of MWCNTs (Figure 2a), displayed a significant peak indexed to (002) crystal plane which appeared at 2θ = 26° corresponding to hexagonal graphite structure of acid treated/functionalised MWCNTs [37]. A similar behaviour was reported by Yuan et al. [29]. The broad peak of PVDF-HFP (Figure 2c) slightly intensified upon addition of 1 wt.% MWCNTs onto PVDF-HFP and the data clearly shows that most of the MWCNTs are encapsulated by a layer of PVDF-HFP. The interlayer peak of PAMAM-MWCNTs (Figure 2d) indicates that the functional materials affected the crystallinity of MWCNTs as the data from TGA (Figure 3) also revealed that 50% of PAMAM was present in MWCNTs. The peak due to PAMAM-MWCNTs slightly intensified on 1 wt.% PAMAM-MWCNTs/PVDF-HFP (Figure 2e), and this is because only 1 wt.% PAMAM-MWCNTs was added to PVDF-HFP, hence its effect was slightly noticed on the XRD pattern.

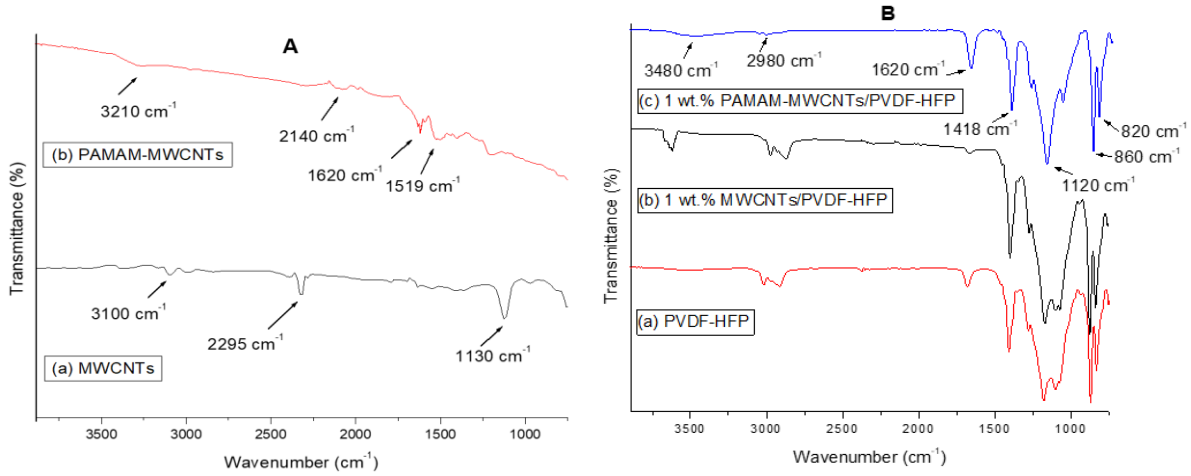

Fig. 1. (A) FTIR spectra of (a) MWCNTs and (b) PAMAM-MWCNTs; **(B)** FTIR spectra of (a) PVDF-HFP, (b) 1 wt.% MWCNTs/PVDF-HFP, and (c) 1 wt.% PAMAM-MWCNTs/PVDF-HFP nanocomposite membranes.

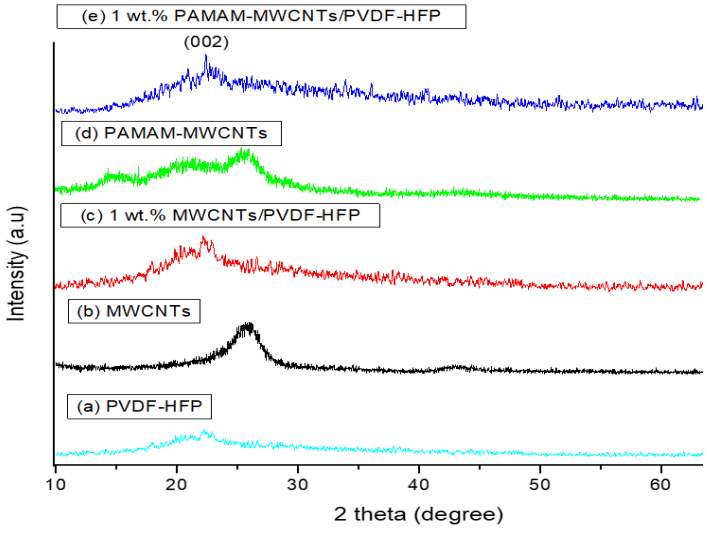

Fig. 2. XRD patterns of (a) PVDF-HFP, (b) MWCNTs (c) 1 wt.% MWCNTs/PVDF-HFP, (d) PAMAM-MWCNTs, and (e) 1 wt.% PAMAM-MWCNTs/PVDF-HFP composite membranes.

3.1.3. TGA profiles of PVDF-HFP, MWCNTs, 1 wt.% MWCNTs/PVDF-HFP, PAMAM-MWCNTs, and 1 wt.% PAMAM-MWCNTs/PVDF-HFP composite membranes

Figure 3 shows the TGA profiles of PVDF-HFP, MWCNTs, 1 wt.% MWCNTs/PVDF-HFP, PAMAM-MWCNTs and 1 wt.% PAMAM-MWCNTs/PVDF-HFP composite membranes. All materials showed weight losses as the temperature increases. The weight loss of MWCNTs (Figure 3(b)) occurred above 500°C, and it's attributed to the loss of the oxygen-containing functional groups of MWCNTs, as observed by Watts et al. [38]. The PVDF-HFP polymeric membrane (Figure 3(a)) showed a first weight loss from 200°C, second weight loss at 350°C, which was followed by third step at 400°C. This clearly shows the instability of PVDF-HFP as compared to MWCNTs. The data indicates that the 1wt.% MWCNTs added on PVDF-HFP is too small to have an impact on the structural stability of PVDF-HFP (Figure 3c), in fact it seems to have slightly weakened the PVDF structure, while improving in other areas such as porosity and contact angle (Table 1).

The TGA profiles of PAMAM-MWCNTs (Figure 3d) shows a 50% weight loss from 240 to 290°C, which can be easily attributed to the decomposition of PAMAM organic moiety substituent. The weight loss of PAMAM-MWCNTs after 300°C is attributed to the thermal decomposition of the defect sites of PAMAM-MWCNTs. Similar weight percentages were observed by Salam and Burk [39]. The 1 wt.% PAMAM-MWCNTs/PVDF-HFP composite membrane (Figure 3e) retained stability up to 500°C, which was then followed by a loss of PAMAM organic species and PVDF-HFP polymeric materials. This further confirms that small amounts of MWCNTs are present on the 1 wt.% PAMAM-MWCNTs/PVDF-HFP composite membrane. The data surprisingly indicates that the combination of both PAMAM and MWCNTs improves the structural stability of PVDF-HFP membrane, which remained stable even at high temperatures when compared to 1 wt.% MWCNTs/PVDF-HFP composite membranes. Related results were observed elsewhere [39], on as-prepared MWCNTs modified with octadecylamine and polyethylene glycol composites.

3.1.4. FIB-SEM images of PVDF-HFP, 1 wt.% MWCNTs/PVDF-HFP, and 1 wt.% PAMAM-MWCNTs/PVDF-HFP composite membranes

Figure 4 shows the FIB-SEM images of the cross section of PVDF-HFP, 1 wt.% MWCNTs/PVDF-HFP and 1 wt.% PAMAM-MWCNTs/PVDF-HFP composite membranes. The cross sections of the membranes exhibited asymmetric structures consisting of a thin dense layer supported by a large finger-like sublayers. The cross-sections of all membranes (Figure 4a1, b1 and c1), exhibited a mixture of finger-like macro-voids and a spongy structure. The macrovoids were decreased on the modified PVDF-HFP (Figure 4b1 and c1), with a high spongy surface which is good for adsorption [40]. It was noticed at high magnification that some of the MWCNTs on 1 wt.% MWCNTs/PVDF-HFP (Figure 4b1), formed agglomerates (shown with arrows) when compared to PVDF-HFP and 1 wt.% PAMAM-MWCNTs/PVDF-HFP composite membranes. These agglomerates can lead to blockages of some pore structures as noticed elsewhere [41], thus lowering the surface area of the membrane as noted by BET data (Table 1). Hence, PAMAM could be playing an important role of evenly distributing MWCNTs on the interior and surface structure of PVDF-HFP [41].

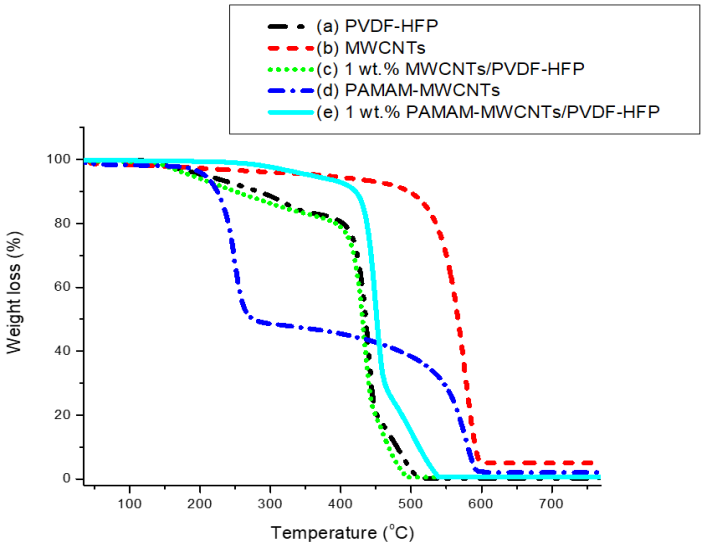

Fig. 3. TGA profiles of (a) PVDF-HFP, (b) MWCNTs (c) 1 wt.% MWCNTs/PVDF-HFP, (d) PAMAM-MWCNTs, and (e) 1 wt.% PAMAM-MWCNTs/PVDF-HFP composite membranes.

Table 1
BET data of PVDF-HFP, MWCNTs, 1 wt.% MWCNTs-PVDF-HFP, PAMAM-MWCNTs and 1 wt.% PAMAM-MWCNTs/PVDF-HFP composite membrane.

Sample name	BET surface area (m^2g^{-1})	Pore volume (cm^3g^{-1})	Contact angle (º)
MWCNTs	239.8	1.797	-
PAMAM-MWCNTs	87.71	0.6687	-
PVDF-HFP	3.608	0.09436	78
1 wt.% MWCNTs-PVDF-HFP	3.772	0.09508	59
1 wt.% PAMAM-MWCNTs/PVDF-HFP	3.975	0.1199	54

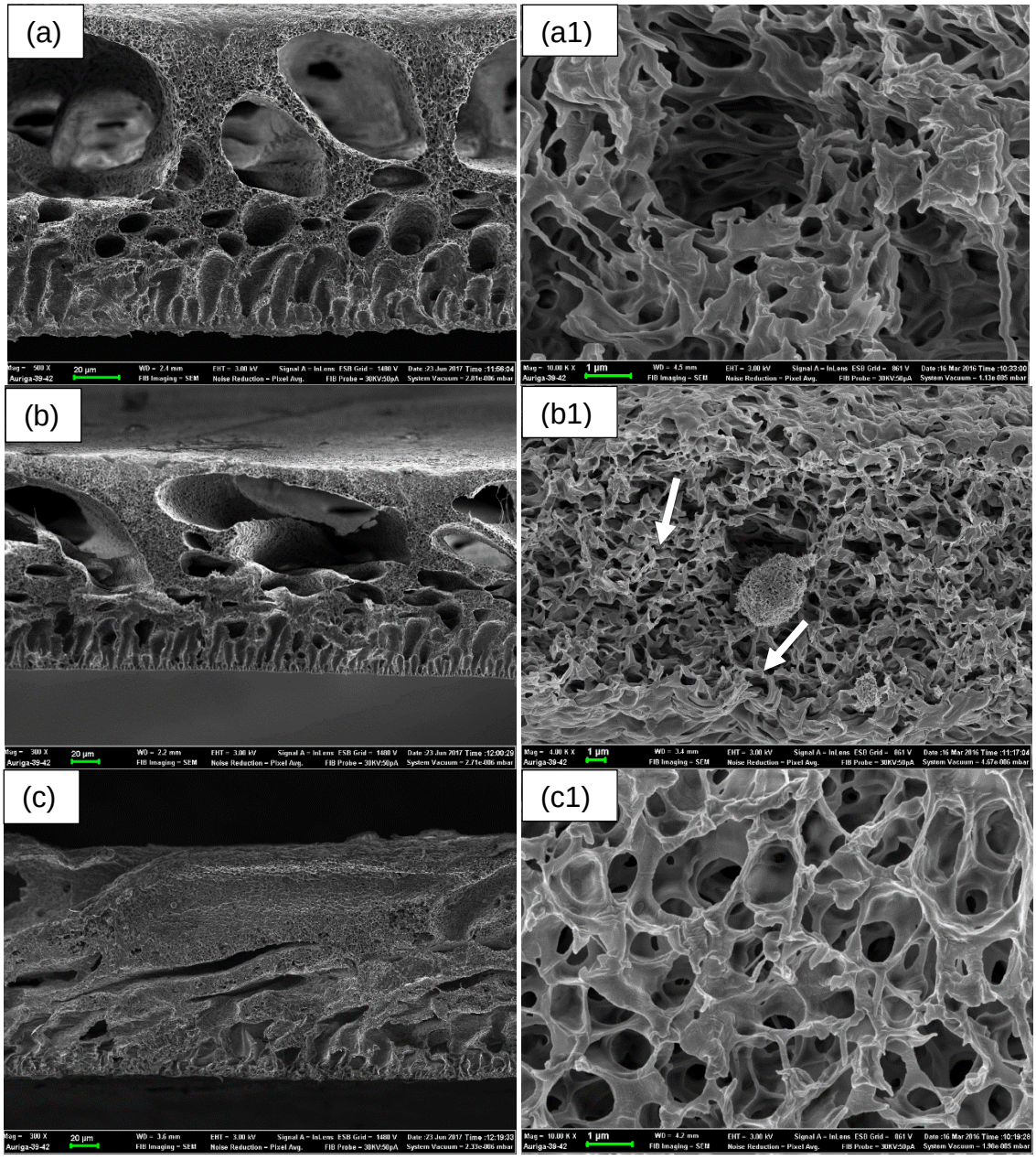

Fig. 4. FIB-SEM cross-sectional images of: (a) PVDF-HFP, (b) 1 wt.% MWCNTs/PVDF-HFP and (c) 1 wt.% PAMAM-MWCNTs/PVDF-HFP composite membranes and their higher magnification cross-sectional images (a1, b1 and c1).

The BET data for MWCNTs, PAMAM-MWCNTs, PVDF-HFP, 1 wt.% MWCNTs/PVDF-HFP, and 1 wt.% PAMAM-MWCNTs/PVDF-HFP composite membranes is presented in Table 1. The BET data indicated that the surface area and pore volume of MWCNTs decreased when PAMAM was introduced on the MWCNTs. It is suggested that the observed decrease in surface area resulted from enhanced interfacial interactions between the PAMAM functional groups and the surface of MWCNTs [42,43]. The BET data shows that the PVDF-HFP of polymeric membrane has lower surface area (3.608 m^2g^{-1}). However, upon modification with either MWCNTs or PAMAM-MWCNTs, the surface area increased. The change in BET surface area is as follows: 1 wt.% PAMAM-MWCNTs/PVDF-HFP > 1 wt.% MWCNTs/PVDF-HFP > PVDF-HFP. The increase in surface area can be linked to opening of pores upon addition of MWCNTs, which further opens up with addition of PAMAM-MWCNTs.

Hydrophilicity studies were done by measuring the contact angle of the membranes as shown in Table 1. The data indicates an improved hydrophilicity of PVDF-HFP upon addition of MWCNTs or PAMAM-MWCNTs [25], which is mainly due to an increase in surface porosity. These results are supported by FIB-SEM surface and cross-section data. Similar results were reported elsewhere [44] after incorporating MWCNTs on polyethersulfone membranes.

4. Adsorption studies

4.1. Effect of pH on Cd(II) ions removal by PVDF-HFP composites membranes

Figure 5 shows the effect of pH on adsorption of Cd(II) by PVDF-HFP, 1 wt.% MWCNTs/PVDF-HFP and 1 wt.% PAMAM-MWCNTs/PVDF-HFP composite membranes. The pH value is considered as one of the main parameters controlling the sorption of metals with adsorbent. The data shows that the adsorption of Cd(II) ions increased from 84.24 to 87.97% as the pH was increased from 4 to 6.5, when using the PVDF-HFP composite membranes. However, at pH higher than 6.5, the Cd(II) ions adsorption decreased in a steep slope. The decrease in adsorption of Cd(II) ions at higher pH is due to precipitation of cadmium hydroxides; forming white crystals [45]. At low pH values, H^+ ions occupy most of the adsorption sites on the membrane surface; hence less Cd(II) ions are adsorbed due to electric repulsion [46]. This study showed that the pH of 6.5 gave the best adsorption

which is close to the neutral pH of water (6.8 - 7); hence, the pH value of 6.5 was selected for the remaining tests.

4.2. Effect of adsorption kinetics of Cd(II) removal by PVDF-HFP composites membranes

Figure 6 shows the effect of contact time on the adsorption efficiency of Cd(II) ions (100 ppm) by PVDF-HFP based membranes. During the first 180 minutes, adsorption of Cd(II) ions increased rapidly after which it became slow when the equilibrium point was reached after 360 minutes. Such behaviour is typically due to the presence of several adsorption sites on the surface of the membrane; in the initial stage of reaction, which gradually gets saturated by Cd(II) ions as the contact time increases. Interestingly, a slight increase was observed when MWCNTs were added on PVDF-HFP. The highest adsorption of 96% was observed on 1 wt.% PAMAM-MWCNTS/PVDF-HFP and the results correlate with BET and contact angle data (Table 1), wherein 1 wt.% PAMAM-MWCNTs/PVDF-HFP composite membrane showed the highest surface area.

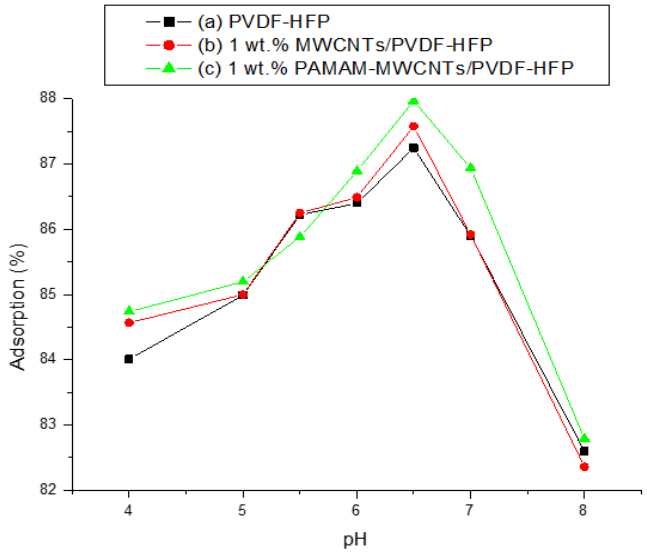

Fig. 5. Effect of pH on the adsorption of Cd(II) ions on (a) PVDF-HFP, (b) 1 wt.% MWCNTs-PVDF-HFP and (c) 1 wt.% PAMAM-MWCNTs/PVDF-HFP composite membranes.

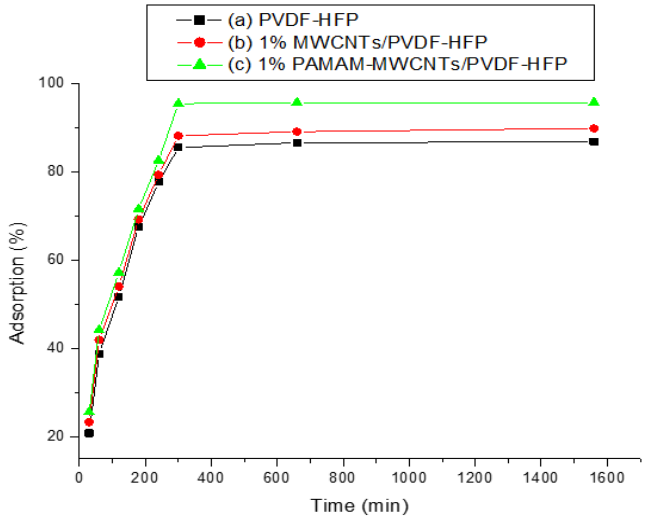

Fig. 6. Effect of contact time on adsorption efficiency of Cd(II) ions by (a) PVDF-HFP, (b) 1 wt.% MWCNTs/PVDF-HFP and (c) 1 wt.% PAMAM-MWCNTs/PVDF-HFP composite membranes.

In order to describe the kinetic behaviour during the adsorption of Cd (II) ion, pseudo-first-order (A), and pseudo-second-order (B), models were used as shown in Figure 7. Figure 6A and 6B show the pseudo first-order and second-order plots of the composite membranes, respectively. The slopes and intercepts of the curves in Figure 7A and B were used to determine k (the constant), q_e (capacity) and R (the corresponding linear regression correlation coefficient) (Table 2).

The data in Table 2 clearly show that the values of experimental q_e were in close agreement with the q_e obtained in pseudo-second-order rate model, indicating the alignment of experimental data to pseudo-second-order rate model. Moreover, the correlation coefficient (R^2=0.997-0.998) confirms the explanation of the suitability of the pseudo-second order kinetic model. Hence, a pseudo-second-order model was considered as an appropriate model [46,47].

4.3. Adsorption isotherms

The data in Figure 8 shows the effect of temperature on the adsorption efficiency of Cd(II) ions by 1 wt.% PAMAM-MWCNTs/PVDF-HFP composite membrane. The results indicate an increase in adsorption efficiency as the Cd(II) ions concentration increases. The adsorption efficiency of the composite at 15°C has shown an exponential growth as the concentration increases. Furthermore, as the temperature is raised, the adsorption efficiency of composite increased by notable margins, with 99% adsorption at 45°C. This may be due to an increase in thermal energy of the adsorbing material, which led to higher adsorption and faster adsorption rate as observed elsewhere [48]. An increase in the initial Cd(II) concentration also improves the interaction between the metal and the adsorbent due to the increase in the driving force of the concentration gradient, which results in higher adsorption [46].

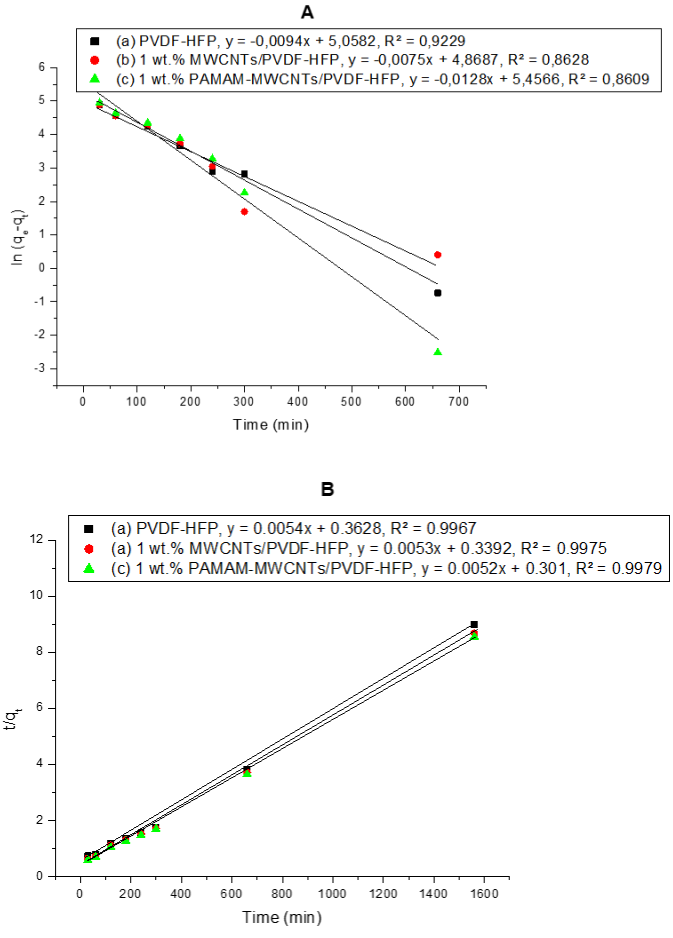

Fig. 7. Pseudo-first order (A) and Pseudo-second order (B) kinetic model for adsorption of Cd (II) ions on (a) PVDF-HFP, (b) 1 wt.% MWCNTs-PVDF-HFP and (c) 1 wt.% PAMAM-MWCNTs-PVDF-HFP composite membrane.

Figure 9 shows the linearized data for the adsorption of Cd(II) ions on 1 wt.% PAMAM-MWCNTs-PVDF-HFP composite membrane by applying Langmuir and Freundlich isotherm model. The isotherm constants and their correlation coefficients (R^2) are listed in Table 3. Based on the R^2 values, the results indicate that the adsorption processes of all composites membranes are well fitted to the Freundlich model, which suggest a multilayer adsorption as reported elsewhere [31,49]. The Freundlich constant, K_f, corresponding to adsorption capacity increased with an increase in temperature, resulting in high adsorption capacity. This is because, as temperature increases, the rate of a chemical reaction increases. The values of n for the adsorption of Cd (II) ions were all close to 1 showing good efficiency for Cd (II) ions on PVDF-HFP [30].

The maximum adsorption capacity from Langmuir equation for 1 wt.% PAMAM-MWCTs/PVDF-HFP composite membrane was 167 mg/g at room temperature, higher than those reported in literature (Table 4). The separation factor, R_L, values were all below 1 indicating favourable adsorption as recorded previously [31,33,49].

Table 2
Kinetics parameters for Cd (II) adsorption onto PVDF-HFP based membranes.

Membrane	q_e (mg/g)	Pseudo-first-order kinetic model			Pseudo-second-order kinetic model		
		K_1 (min^{-1})	q_e (mg/g)	R^2	K_2 (g/mg·min)	q_e (mg/g)	R^2
PVDF-HFP membrane	173.82	0.0094	157.3	0.923	8.04 x 10^{-5}	185.2	0.997
1 wt.% MWCNTs-PVDF-HFP	179.88	0.0075	130.2	0.863	8.28 x 10^{-5}	188.7	0.998
1 wt.% PAMAM-MWCNTs-PVDF-HFP	191.64	0.00128	234.3	0.861	8.98 x 10^{-5}	192.3	0.998

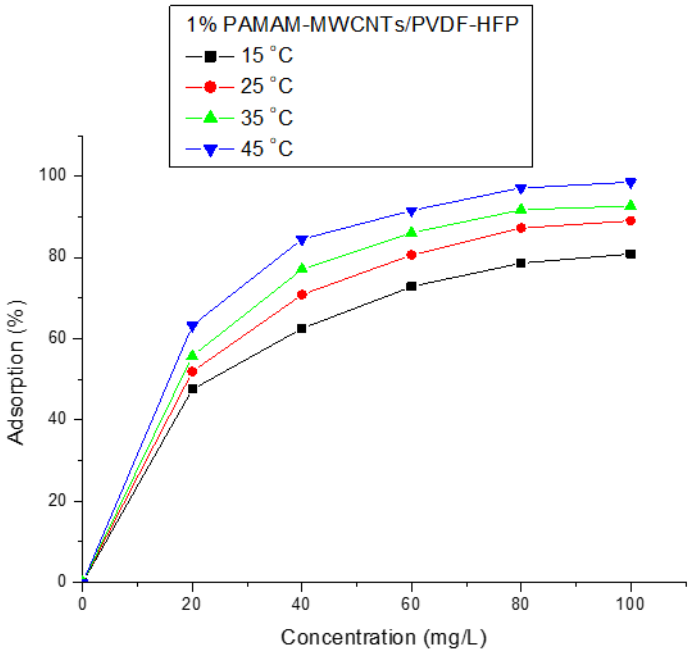

Fig. 8. Effect of temperature on adsorption efficiency of Cd(II) ions on 1 wt.% PAMAM-MWCNTs/PVDF-HFP composite membrane.

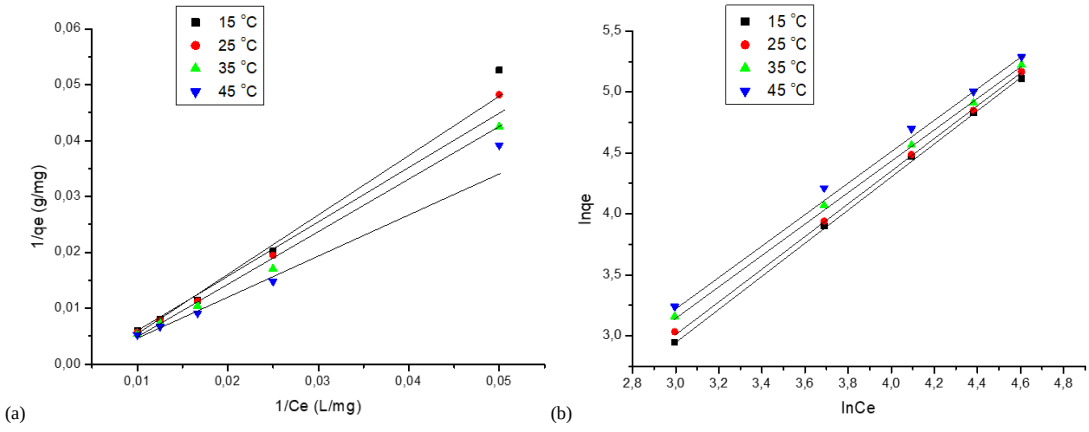

Fig. 9. (a) Langmuir and (b) Freundlich isotherm of Cd(II) ions adsorption on 1 wt.% PAMAM-MWCNTs/PVDF-HFP composite membrane.

Table 3
Langmuir and Freundlich isotherm parameters for Cd(II) ions adsorption onto PVDF 1 wt.% PAMAM-MWCNTs/PVDF-HFP composite membrane.

Temperature (°C)	Langmuir model				Freundlich model		
	q_m (mg/g)	b (L/mg)	R^2	R_L	K_f (mg/g)	N	R^2
15	137	0.00619	0.994	0.618	0.338	0.74	0.999
25	166.7	0.00556	0.997	0.643	0.394	0.76	0.999
35	212.8	0.00504	0.996	0.665	0.53	0.79	0.999
45	323	0.00360	0.991	0.735	0.604	0.80	0.997

Table 4
Comparison of Cd(II) ions adsorption capacity by different materials.

Adsorbent	Experimental conditions			Adsorption capacity Qmax (mg/g)	Reference
	pH	T (°C)	Dosage		
1wt.% PAMAM-MWCNTs/ PVDFHFP	6.5	298	0.5 g/L	167	this study
Mesoporous silica nano-composite materials	5.5	298	1 g/L	148.32	[50]
Surfactant-modified chitosan beads	7.0	298	0.45 g/L	125	[7]
Aluminum Oxide-Impregnated Carbon Nanotube Membrane	7.0	298	Not specified	54.42	[51]
Poly(sodium 4-styrenesulfonate) -grafted polysulfone Porphyrin p-toluenesulfonate (PSF-PNaSS/ TMPyP)	8.0	298	Not specified	72.2	[52]
Graphene oxide/cellulose membranes	4.5	298	Not specified	26.8	[53]
Graphene oxide membranes	5.8	303	0.2 g/L	83.8	[54]
Graphene oxide nanosheets	4.99	298	0.5 g/L	44.64	[55]
PVDF/Graphene Oxide Nanofiber Composite Membranes	7	298	Not specified	1.11	[56]

4.4. Adsorption thermodynamics

Figure 10 shows the linear plot of InK_o vs 1/T for Cd(II) on PVDF-HFP based membranes at different concentrations. The Arrhenius plot is obtained by plotting the logarithm of the rate constant, k, versus the inverse temperature, 1/T. The resulting negatively-sloped line is useful in finding the missing components of the Arrhenius equation. The values of ΔH^o and ΔS^o were obtained from the slope and intercept of the plot of InK_o versus 1/T. A similar trend was also reported in literature [57].

The thermodynamics parameters, ΔG^o, ΔH^o, and ΔS^o were calculated from the slopes and intercept of the Van't Hoff plot as shown in Figure 10 and the data are as summarised in Table 5. The values of ΔG^o decreased from -5.397 to -10.45 as the temperature increase, indicating that the adsorption process was spontaneously in nature. The positive value of ΔH^o confirmed that the adsorption process was endothermic in nature [47,57,58]. A higher temperature is favourable to the adsorption, which may explain the increase in q_{max} on Langmuir isotherm as the temperature is raised. The positive value of ΔS^o reflected an increase in randomness at the adsorbent-solution interface during the Cd(II) ions adsorption process as observed in literature. The data indicates that the adsorption process of Cd(II) ions by 1 wt.% PAMAM-MWCNTs/PVDF-HFP composite membrane is spontaneous, endothermic and mainly physical in nature [18,48].

4.5. Reusability studies

Figure 11 shows the reusability studies of PVDF-HFP, 1 wt.% MWCNTs-PVDF-HFP and 1 wt.% PAMAM-MWCNTs/PVDF-HFP composite membranes on adsorption of Cd(II) ions. Reusability is one of the vital aspects for the practical application of the adsorbent. The adsorption capacity from the first to the fourth cycle decreased from 91 to 83%, 95 to 87% and 98 to 93 % for PVDF-HFP, 1 wt.% MWCNTs/PVDF-HFP and 1 wt.% PAMAM-MWCNTs/PVDF-HFP composite membranes, respectively. The PVDF-HFP and 1 wt.% MWCNTs-PVDF-HFP had the highest adsorption capacity loss as compared to 1 wt.% PAMAM-MWCNTs/PVDF-HFP composite membrane. However, the adsorption capacity of the two composites remained above 80% after four cycles, which indicates that PVDF-HFP adsorbents can be recycled for Cd (II) ions adsorption. The adsorption loss for 1 wt.% PAMAM-MWCNTs/PVDF-HFP composite membrane after 4 cycles was 5% compared to the adsorption loss of 12% observed by Wang et al. [59].

Table 5
Thermodynamic parameters for Cd (II) (100 ppm) adsorption by 1 wt.% PAMAM-MWCNTs/PVDF-HFP.

Temperature (K)	Thermodynamic parameters		
	ΔG (kJ.mol^{-1})	ΔH (kJ.mol^{-1})	ΔS (J.mol.K^{-1})
288	-5,397	41.87	163.19
298	-6,559		
308	-7,896		
318	-10,45		

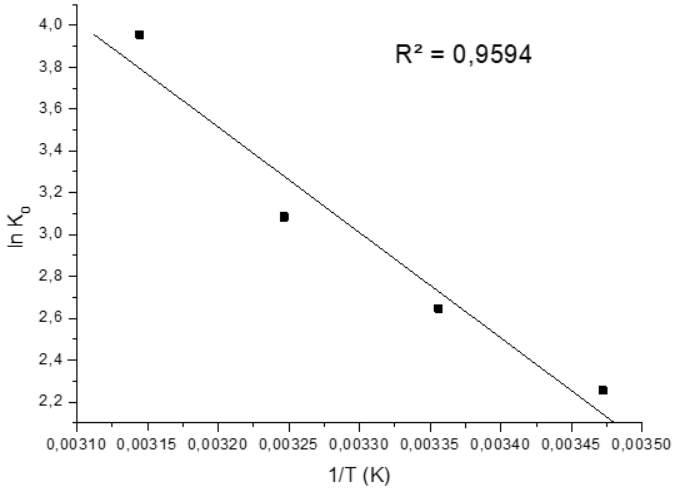

Fig. 10. Thermodynamics parameters of Cd(II) ions onto 1 wt.% PAMAM-MWCNTs/PVDF-HFP.

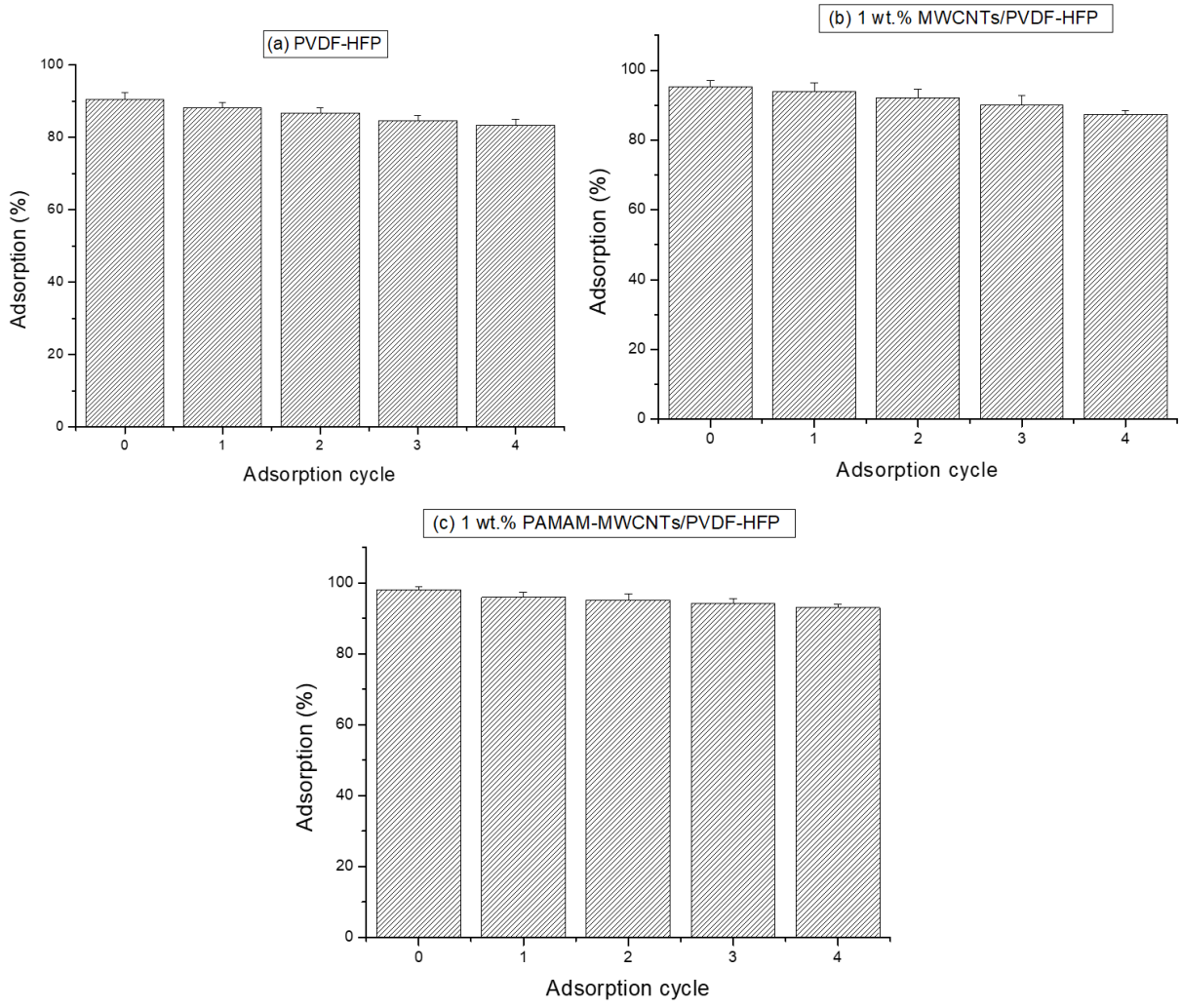

Fig. 11. Reusability of (a) PVDF-HFP, (b) 1 wt.% MWCNTs/PVDF-HFP and (c) 1 wt.% PAMAM-MWCNTs/PVDF-HFP composite membrane on the adsorption of Cd(II) ions.

To validate that some Cd(II) ions remained strongly adsorbed on the 1 wt.% PAMAM-MWCNTs/PVDF-HFP composite membrane, the re-used membranes were analysed by ICP-OES. The 1 wt.% PAMAM-MWCNTs/PVDF-HFP composite membrane samples were digested in 2% HNO_3 and analysed for Cd(II) ions. The analysis showed that 1.8, 2.5, 2.7 and 4.75% Cd(II) ions remained strongly attached to membrane after reusing the membranes 4 times, respectively. This data supports the observed decrease in adsorption capacity, due to the loss of the adsorption sites as the reusability cycle increases (Figure 10).

Figure 12 shows the SEM images, contact angles and EDX data of used and cleaned (a1, 1 wt.% PAMAM-MWCNTs/PVDF-HFP composite membrane. The SEM data show that the morphology remains unchanged both before (Figure 11a) and after reusing the membrane (Figure 11e). The contact angles of PVDF-HFP composite membranes increased after Cd(II) ions adsorption indicating a reduction in hydrophilicity. The increase in hydrophilicity was noticed after cleaning the composite membranes showing the effectiveness of membrane cleaning for reusability purposes. On average, the membranes hydrophilicity did not significantly change after reusing the membrane when compared to the data in Table 1. EDX showed less percentage of Cd(II) ions on the surface of the membrane (most of it adsorbed within the membrane) after adsorption and none metal was detected on the surface after cleaning the membranes. Carbon, fluorine and oxygen which are the major constituents of PVDF-HFP were all retained on the membrane surface during the whole reusability process, further confirming the stability and good reusability of the 1 wt.% PAMAM/PVDF-HFP composite membrane.

4.6. Selectivity studies

Figure 13 shows the competitive adsorption studies of cadmium ions by 1 wt.% PAMAM-MWCNTs/PVDF-HFP composite membrane on binary and quaternary metal solutions. To investigate the selectivity of 1 wt.% PAMAM-MWCNTs/PVDF-HFP composite membrane in adsorption studies; solutions of Cd(II)/Cu(II), Cd(II)/Zn(II), and Cd(II)/Ni(II) binary mixtures were used. The data in Figure 13 indicates that the adsorption capacity of Cd (II) in the binary solutions decreased slightly, as compared to the adsorptions of cadmium alone. However, the adsorption remained high (91%) as compared to that of copper (II) (56%), Zinc (II) (51%) and Nickel (II) (48%) and similar results were reported elsewhere [60]. The same sequence was noted in quaternary solutions, where in the order was as follows: Cd(II)>Cu(II) > Zn(II) > Ni(II). This selectivity data is supported by Irving-Williams series, which indicates that the relative stabilities of complexes formed by the transition metal ions with ligands follows the sequence: Cu(II) > Zn(II) > Ni(II) [61]. The adsorption by 1 wt.% PAMAM-MWCNTs/PVDF-HFP composite membrane was more selective towards Cd(II) ions than other metals because adsorption conditions such as pH was optimised for Cd (II) ions adsorption only.

The selectivity parameters of Cd(II) in the Cd/Cu, Cd/Zn and Cd/Ni binary solution are given in Table 6. Based on the distribution coefficient values (K_d), the adsorption capacity of all composite membranes were more selective towards Cd(II) [60]. The 1 wt.% PAMAM-MWCNTs/PVDF-HFP composite membrane exhibited higher selectivity coefficients (K) towards Cd(II) in Cu(II), Zn(II) and Ni(II) in binary metal solutions.

Table 6
Selectivity parameters for 1 wt.% PAMAM-MWCNTs/PVDF-HFP membrane on Cadmium (II), Copper (II), Zinc (II) and Nickel (II) binary solutions.

Metals	K_d(Cd)	K_d(X)	K
Cd(II)/Cu(II)[a]	10.2	2.54	4.02
Cd(II)/Zn(II)[a]	9.5	2.09	4.55
Cd(II)/Ni(II)[a]	8.7	1.82	4.78

[a] All competitor ions have the same charge, with more or less similar ionic radius with Cd(II) ion and adsorb at pH between 6 and 7.

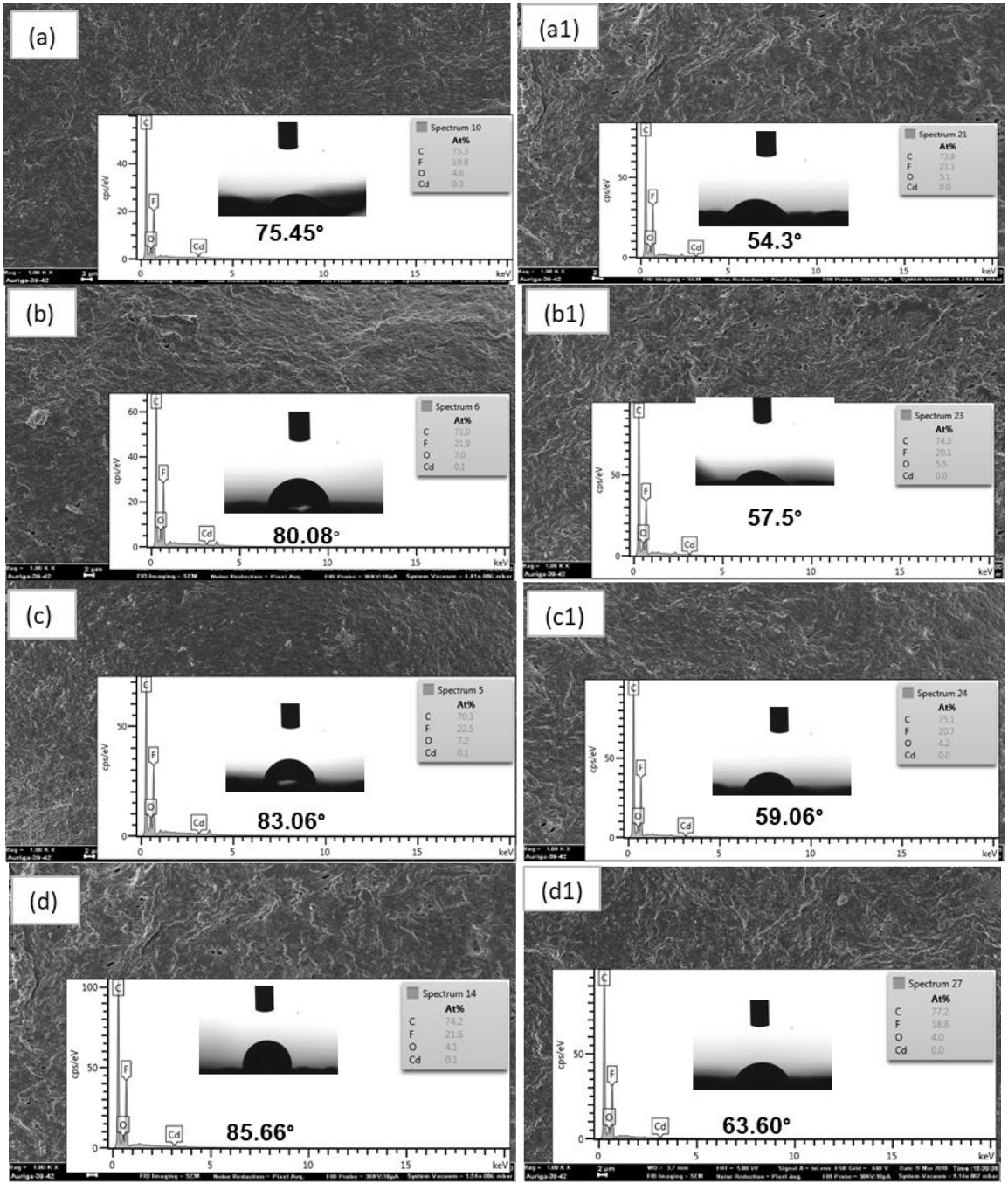

Fig. 12. SEM images, contact angles and EDX data of used (a, b, c and d) and cleaned (a1, b1, c1 and d1), 1 wt.% PAMAM-MWCNTs/PVDF-HFP composite membrane.

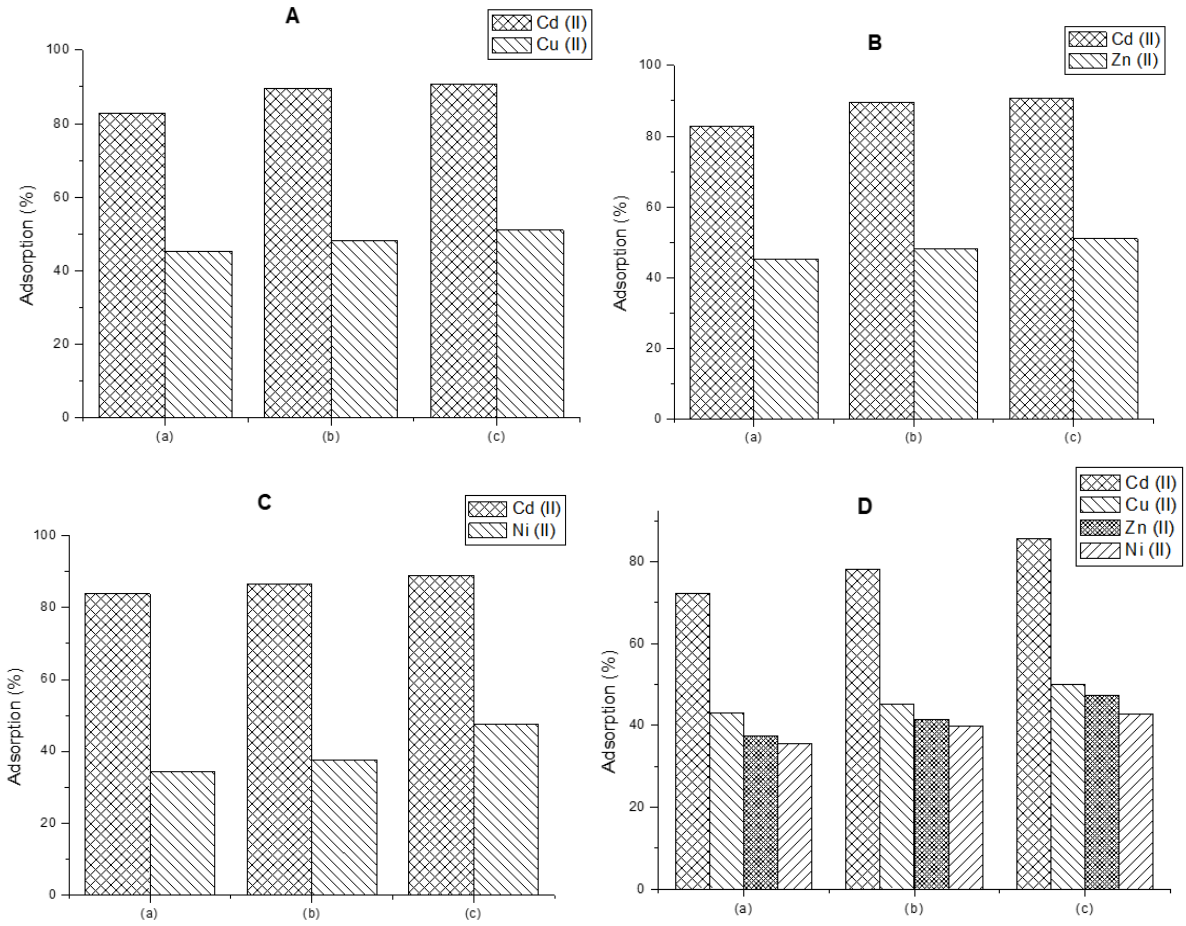

Fig. 13. Competitive adsorption studies of cadmium ions by (a) PVDF-HFP, (b) 1 wt.% MWCNTs-PVDF-HFP and (c) 1 wt.% PAMAM-MWCNTs-PVDF-HFP on (A) Cd(II)/Cu(II), (B) Cd(II)/Zn(II), (C) Cd(II)/Ni(II) binary and (D) Cd(II)/Cu(II)/Zn(II)/Ni(II) quaternary metal solutions.

5. Conclusions

PVDF-HFP composite membranes with high adsorption performance towards Cd(II) ions were successfully prepared by phase inversion method. FTIR data confirmed the existence of PAMAM-MWCNTs on the surface of the PVDF-HFP composite membranes. TGA data demonstrated that the thermal stability of the composite membranes was enhanced by the addition of PAMAM-MWCNTs. The SEM images of PVDF-HFP composite membranes showed a decrease in the microvoids, with a high spongy surface which is excellent for heavy metal adsorption. BET data revealed that the surface area, pore volume and pore sizes of composite membranes were improved upon blending with PAMAM-MWCNTs. The composite membranes could optimally adsorb Cd(II) ions, at a pH of 6.5. The equilibrium data fitted well with the Freundlich isotherm model, and the maximum Langmuir adsorption capacity of 1 wt.% PAMAM-MWCNTs/PVDF-HFP composite membrane was 167 mg/g at 25°C. The thermodynamic analysis confirmed that the adsorption process was spontaneous, while ΔH^o and ΔS^o positive values indicated that the adsorption was endothermic in nature. The 1 wt.% PAMAM-MWCNTs/PVDF-HFP composite membrane can be reused at least 4 times, with an adsorption loss of less than 5%, as confirmed by ICP-OES analysis. Furthermore, the composite membrane was highly selective towards Cd(II) ions in the binary metal adsorption solutions.

Acknowledgements

The authors greatly acknowledge the financial support from National Research Foundation (NRF). The authors would also like to thank University of Limpopo, department of Chemistry and department of Biochemistry, Microbiology and Biotechnology for providing support for this research work.

References

[1] F. Fu, Q. Wang, Removal of heavy metal ions from wastewaters: A review, J. Environ. Manage. 92 (2011) 407–418. https://doi.org/10.1016/j.jenvman.2010.11.011.

[2] P.F. Gomes, P.R. Lennartsson, N.K. Persson, M.J. Taherzadeh, Heavy metal biosorption by rhizopus Sp. biomass immobilized on textiles, Water. Air. Soil Pollut. 225 (2014). https://doi.org/10.1007/s11270-013-1834-4.

[3] S.K.R. Yadanaparthi, D. Graybill, R. von Wandruszka, Adsorbents for the removal of arsenic, cadmium, and lead from contaminated waters, J. Hazard. Mater. 171 (2009) 1–15. https://doi.org/10.1016/j.jhazmat.2009.05.103.

[4] A.T. Ojedokun, O.S. Bello, Sequestering heavy metals from wastewater using cow dung, Water Resour. Ind. 13 (2016) 7–13. https://doi.org/10.1016/j.wri.2016.02.002.

[5] Q. Li, H. Liu, M. Alattar, S. Jiang, J. Han, Y. Ma, C. Jiang, The preferential accumulation of heavy metals in different tissues following frequent respiratory exposure to PM2.5 in rats, Sci. Rep. 5 (2015) 1–8. https://doi.org/10.1038/srep16936.

[6] M. Jaishankar, T. Tseten, N. Anbalagan, B.B. Mathew, K.N. Beeregowda, Toxicity, mechanism and health effects of some heavy metals, Interdiscip. Toxicol. 7 (2014) 60–72. https://doi.org/10.2478/intox-2014-0009.

[7] P. Pal, A. Pal, Surfactant-modified chitosan beads for cadmium ion adsorption, Int. J. Biol. Macromol. 104 (2017) 1548–1555. https://doi.org/10.1016/j.ijbiomac.2017.02.042.

[8] M. Rafati Rahimzadeh, M. Rafati Rahimzadeh, S. Kazemi, A.-A. Moghadamnia, Cadmium toxicity and treatment: An update., Casp. J. Intern. Med. 8 (2017) 135–145. https://doi.org/10.22088/cjim.8.3.135.

[9] V.S. Arroyo, K.M. Flores, L.B. Ortiz, L.E. Gómez-quiroz, M.C. Gutiérrez-ruiz, Journal of Drug Metabolism &, (2012) 1–7. https://doi.org/10.4172/2157-7609.S5-001.

[10] SANS 241-1 : 2015 SOUTH AFRICAN NATIONAL STANDARD Drinking water Part 1 : Microbiological, physical, aesthetic, in: 2015.

[11] T. Dalgleish, J.M.G.. Williams, A.-M.J. Golden, N. Perkins, L.F. Barrett, P.J.

Barnard, C. Au Yeung, V. Murphy, R. Elward, K. Tchanturia, E. Watkins, Health risks of heavy metals from long-range transboundary air pollution, 2007.

[12] T. Macek, M. Mackova, Potential of Biosorption Technology, (n.d.) 7–18. https://doi.org/10.1007/978-94-007-0443-5.

[13] N. Das, R. Vimala, P. Karthika, Biosorption of heavy metals - An overview, Indian J. Biotechnol. 7 (2008) 159–169. https://doi.org/10.1016/j.is.2009.02.003.

[14] A.E. Burakov, E. V. Galunin, I. V. Burakova, A.E. Kucherova, S. Agarwal, A.G. Tkachev, V.K. Gupta, Adsorption of heavy metals on conventional and nanostructured materials for wastewater treatment purposes: A review, Ecotoxicol. Environ. Saf. 148 (2018) 702–712. https://doi.org/10.1016/j.ecoenv.2017.11.034.

[15] H. Yaacoubi, O. Zidani, M. Mouflih, M. Gourai, S. Sebti, Removal of Cadmium from water using Natural phosphate as Adsorbent, Procedia Eng. 83 (2014) 386–393. https://doi.org/10.1016/j.proeng.2014.09.039.

[16] M.A. Barakat, New trends in removing heavy metals from industrial wastewater, Arab. J. Chem. 4 (2011) 361–377. https://doi.org/10.1016/j.arabjc.2010.07.019.

[17] K. Tohdee, Kaewsichan, Lupong, U. Asad, Enhancement of adsorption efficiency of heavy metal Cu(II) and Zn(II) onto cationic surfactant modified bentonite, Biochem. Pharmacol. 6 (2018) 2821–2828. https://doi.org/10.1016/j.jece.2018.04.030.

[18] V. Ganesan, C. Louis, S.P. Damodaran, Graphene oxide-wrapped magnetite nanoclusters: A recyclable functional hybrid for fast and highly efficient removal of organic dyes from wastewater, J. Environ. Chem. Eng. 6 (2018) 2176–2190. https://doi.org/10.1016/j.jece.2018.03.026.

[19] A. Ahmad, M.H. Razali, M. Mamat, F.S.B. Mehamod, K. Anuar Mat Amin, Adsorption of methyl orange by synthesized and functionalized-CNTs with 3-aminopropyltriethoxysilane loaded TiO2nanocomposites, Chemosphere. 168 (2017) 474–482. https://doi.org/10.1016/j.chemosphere.2016.11.028.

[20] D. Zhao, J.P. Chen, Application of Zirconium/PVA Modified Flat-Sheet PVDF Membrane for the Removal of Phosphate from Aqueous Solution, Ind. Eng. Chem. Res. 55 (2016) 6835–6844. https://doi.org/10.1021/acs.iecr.6b00186.

[21] D. Zhao, Y. Yu, J.P. Chen, Treatment of lead contaminated water by a PVDF membrane that is modified by zirconium, phosphate and PVA, Water Res. 101 (2016) 564–573. https://doi.org/10.1016/j.watres.2016.04.078.

[22] R.M. Nthumbi, A.A. Adelodun, J.C. Ngila, Electrospun and functionalized PVDF/PAN composite for the removal of trace metals in contaminated water, Phys. Chem. Earth. 100 (2017) 225–235. https://doi.org/10.1016/j.pce.2016.08.007.

[23] B. Hayati, A. Maleki, F. Najafi, H. Daraei, F. Gharibi, G. McKay, Synthesis and characterization of PAMAM/CNT nanocomposite as a super-capacity adsorbent for heavy metal (Ni2 +, Zn2 +, As3 +, Co2 +) removal from wastewater, J. Mol. Liq. 224 (2016) 1032–1040. https://doi.org/10.1016/j.molliq.2016.10.053.

[24] A.M. Stephan, S.G. Kumar, N.G. Renganathan, M.A. Kulandainathan, Characterization of poly(vinylidene fluoride-hexafluoropropylene) (PVdF-HFP) electrolytes complexed with different lithium salts, Eur. Polym. J. 41 (2005) 15–21. https://doi.org/10.1016/j.eurpolymj.2004.09.001.

[25] L.E. Macevele, K.L.M. Moganedi, T. Magadzu, Investigation of antibacterial and fouling resistance of silver and multi-walled carbon nanotubes doped poly(Vinylidene fluoride-co-hexafluoropropylene) composite membrane, Membranes (Basel). 7 (2017). https://doi.org/10.3390/membranes7030035.

[26] L.E. Rananga, T. Magadzu, Interaction of silver doped carbon nanotubes-cyclodextrin nanocomposites with Escherichia coli bacteria during water purification, Water Sci. Technol. Water Supply. 14 (2014) 367–375. https://doi.org/10.2166/ws.2013.204.

[27] C. Zhao, L. Ji, H. Liu, G. Hu, S. Zhang, M. Yang, Z. Yang, Functionalized carbon nanotubes containing isocyanate groups, J. Solid State Chem. 177 (2004) 4394–4398. https://doi.org/10.1016/j.jssc.2004.09.036.

[28] B. Pan, D. Cui, F. Gao, R. He, Growth of multi-amine terminated poly(amidoamine) dendrimers on the surface of carbon nanotubes, Nanotechnology. 17 (2006) 2483–2489. https://doi.org/10.1088/0957-4484/17/10/008.

[29] W. Yuan, G. Jiang, J. Che, X. Qi, R. Xu, M.W. Chang, Y. Chen, S.Y. Lim, J. Dai, M.B. Chan-park, Deposition of silver nanoparticles on multiwalled carbon nanotubes grafted with hyperbranched poly amidoamine) and their antimicrobial effects, J. Phys. Chem. B. 112 (2008) 18754–18759. https://doi.org/10.1021/jp807133j.

[30] B. Meroufel, O. Benali, M. Benyahia, Y. Benmoussa, M.A. Zenasni, Adsorptive removal of anionic dye from aqueous solutions by Algerian kaolin: Characteristics, isotherm, kinetic and thermodynamic studies, J. Mater. Environ. Sci. 4 (2013) 482–491. https://doi.org/10.5829/idosi.ijee.2015.06.02.11.

[31] A.S. Bhatt, P.L. Sakaria, M. Vasudevan, R.R. Pawar, N. Sudheesh, H.C. Bajaj, H.M. Mody, Adsorption of an anionic dye from aqueous medium by organoclays: equilibrium modeling, kinetic and thermodynamic exploration, RSC Adv. 2 (2012) 8663. https://doi.org/10.1039/c2ra20347b.

[32] X. Wang, C. Chen, J. Li, X. Wang, Ozone degradation of 1-naphthol on multiwalled carbon nanotubes/iron oxides and recycling of the adsorbent, Chem. Eng. J. 262 (2015) 1303–1310. https://doi.org/10.1016/j.cej.2014.10.107.

[33] M. Rahman, S. Gul, M. Ajmal, A. Iqbal, A.K.K. Achakzai, Removal of cadmium from aqueous solutions using excised leaves of Quetta pine (Pinus halepensis Mill.), Bangladesh J. Bot. 43 (2014) 277–281.

[34] L.E. Rananga, T. Magadzu, Interaction of silver doped carbon nanotubes-cyclodextrin nanocomposites with Escherichia coli bacteria during water purification, Water Sci. Technol. Water Supply. (2014). https://doi.org/10.2166/ws.2013.204.

[35] Y. Zhang, X. Liu, L. Li, Z. Guo, Z. Xue, X. Lu, An electrochemical paracetamol sensor based on layer-by-layer covalent attachment of MWCNTs and a G4.0 PAMAM modified GCE, Anal. Methods. 8 (2016) 2218–2225. https://doi.org/10.1039/C5AY03241E.

[36] Y. Fan, F. Su, K. Li, C. Ke, Y. Yan, Carbon nanotube filled with magnetic iron oxide and modified with polyamidoamine dendrimers for immobilizing lipase toward application in biodiesel production, Sci. Rep. 7 (2017) 1–13. https://doi.org/10.1038/srep45643.

[37] S. Sagar, N. Iqbal, A. Maqsood, Dielectric, electric and thermal properties of carboxylic functionalized multiwalled carbon nanotubes impregnated polydimethylsiloxane nanocomposite, J. Phys. Conf. Ser. 439 (2013). https://doi.org/10.1088/1742-6596/439/1/012024.

[38] P.C.P. Watts, S.J. Henley, E. Mendoza, S.R.P. Silva, J.K. Irvine, E.T. McAdams, Core-shell silver/silver chloride nanoparticles on carbon nanofibre arrays for bio-potential monitoring, Nanotechnology. 18 (2007). https://doi.org/10.1088/0957-4484/18/20/205502.

[39] M.A. Salam, R. Burk, Synthesis and characterization of multi-walled carbon nanotubes modified with octadecylamine and polyethylene glycol, Arab. J. Chem. 10 (2017) S921–S927. https://doi.org/10.1016/j.arabjc.2012.12.028.

[40] X. Zhang, Y. Qin, G. Zhang, Y. Zhao, C. Lv, X. Liu, L. Chen, Preparation of PVDF/hyperbranched-nano- palygorskite composite membrane for efficient removal of heavy metal ions, Polymers (Basel). 11 (2019). https://doi.org/10.3390/polym11010156.

[41] B. Gohari, N. Abu-Zahra, Polyethersulfone Membranes Prepared with 3-Aminopropyltriethoxysilane Modified Alumina Nanoparticles for Cu(II) Removal from Water, ACS Omega. 3 (2018) 10154–10162. https://doi.org/10.1021/acsomega.8b01024.

[42] N. El Badawi, A.R. Ramadan, A.M.K. Esawi, M. El-Morsi, Novel carbon nanotube-cellulose acetate nanocomposite membranes for water filtration applications, Desalination. 344 (2014) 79–85. https://doi.org/10.1016/j.desal.2014.03.005.

[43] H.A. Shawky, S.R. Chae, S. Lin, M.R. Wiesner, Synthesis and characterization of a carbon nanotube/polymer nanocomposite membrane for water treatment, Desalination. 272 (2011) 46–50. https://doi.org/10.1016/j.desal.2010.12.051.

[44] A. Rahimpour, M. Jahanshahi, S. Khalili, A. Mollahosseini, A. Zirepour, B. Rajaeian, Novel functionalized carbon nanotubes for improving the surface properties and performance of polyethersulfone (PES) membrane, Desalination. 286 (2012) 99–107. https://doi.org/10.1016/j.desal.2011.10.039.

[45] S. Wu, K. Zhang, X. Wang, Y. Jia, B. Sun, T. Luo, F. Meng, Z. Jin, D. Lin, W. Shen, L. Kong, J. Liu, Enhanced adsorption of cadmium ions by 3D sulfonated reduced graphene oxide, Chem. Eng. J. 262 (2015) 1292–1302. https://doi.org/10.1016/j.cej.2014.10.092.

[46] P.S. Kumar, S. Ramalingam, V. Sathyaselvabala, S.D. Kirupha, A. Murugesan, S. Sivanesan, Removal of cadmium(II) from aqueous solution by agricultural waste cashew nut shell, Korean J. Chem. Eng. 29 (2012) 756–768. https://doi.org/10.1007/s11814-011-0259-2.

[47] H.N. Tran, S.J. You, H.P. Chao, Thermodynamic parameters of cadmium adsorption onto orange peel calculated from various methods: A comparison study, J. Environ. Chem. Eng. 4 (2016) 2671–2682. https://doi.org/10.1016/j.jece.2016.05.009.

[48] Z. Li, W. Kang, N. Wei, J. Qiu, C. Sun, B. Cheng, Preparation of a polyvinylidene fluoride tree-like nanofiber mat loaded with manganese dioxide for highly efficient lead adsorption, RSC Adv. 7 (2017) 8220–8229. https://doi.org/10.1039/C6RA27865E.

[49] Akl M. Awwad, Biosorption of copper(II) and lead(II) ions from aqueous solutions by modified loquat (Eriobotrya japonica) leaves (MLL), J. Chem. Eng. Mater. Sci. 3 (2012) 7–17. https://doi.org/10.5897/JCEMS11.061.

[50] M.R. Awual, M. Khraisheh, N.H. Alharthi, M. Luqman, A. Islam, M. Rezaul Karim, M.M. Rahman, M.A. Khaleque, Efficient detection and adsorption of cadmium(II) ions using innovative nano-composite materials, Chem. Eng. J. 343 (2018) 118–127. https://doi.org/10.1016/j.cej.2018.02.116.

[51] Ihsanullah, F. Patel, M. Khraisheh, M.A. Atieh, T. Laoui, Novel aluminum oxide-impregnated carbon nanotube membrane for the removal of cadmium from aqueous solution, Materials (Basel). 10 (2017). https://doi.org/10.3390/ma10101144.

[52] L. Zhao, M. Li, M. Liu, Y. Zhang, C. Wu, Y. Zhang, Porphyrin-functionalized porous polysulfone membrane towards an optical sensor membrane for sorption and detection of cadmium(II), J. Hazard. Mater. 301 (2016) 233–241. https://doi.org/10.1016/j.jhazmat.2015.08.044.

[53] E.T. and A.G. Rafal Sitko, Marcin Musielak, Beata Zawisza, Graphene oxide/cellulose membranes in adsorption of divalent metal ions - RSC Advances (RSC Publishing) DOI_10, (n.d.).

[54] P. Tan, J. Sun, Y. Hu, Z. Fang, Q. Bi, Y. Chen, J. Cheng, Adsorption of Cu^{2+}, $Cd^{2+}$and $Ni^{2+}$from aqueous single metal solutions on graphene oxide membranes, J. Hazard. Mater. 297 (2015) 251–260. https://doi.org/10.1016/j.jhazmat.2015.04.068.

[55] X. Xue, J. Xu, S.A. Baig, X. Xu, Synthesis of graphene oxide nanosheets for the removal of Cd(II) ions from acidic aqueous solutions, J. Taiwan Inst. Chem. Eng. 59 (2016) 365–372. https://doi.org/10.1016/j.jtice.2015.08.019.

[56] H. Jeong, W. Jang, J. Yun, H. Byun, Preparation of PVdF/GO Nanofiber Composite Membranes and its Heavy Metal Removal Characteristics, Polym. Korea. 40 (2016) 489–497. https://doi.org/http://dx.doi.org/10.7317/pk.2016.40.3.489.

[57] A. Mohamed, W.S. Nasser, T.A. Osman, M.S. Toprak, M. Muhammed, A. Uheida, Removal of chromium (VI) from aqueous solutions using surface modified composite nanofibers, J. Colloid Interface Sci. 505 (2017) 682–691. https://doi.org/10.1016/j.jcis.2017.06.066.

[58] E. Salehi, S.S. Madaeni, F. Heidary, Dynamic adsorption of Ni(II) and Cd(II) ions

from water using 8-hydroxyquinoline ligand immobilized PVDF membrane: Isotherms, thermodynamics and kinetics, Sep. Purif. Technol. 94 (2012) 1–8. https://doi.org/10.1016/j.seppur.2012.04.004.

[59] D. Wang, L. Liu, X. Jiang, J. Yu, X. Chen, Adsorption and removal of malachite green from aqueous solution using magnetic β-cyclodextrin-graphene oxide nanocomposites as adsorbents, Colloids Surfaces A Physicochem. Eng. Asp. 466 (2015) 166–173. https://doi.org/10.1016/j.colsurfa.2014.11.021.

[60] Q. Kong, B. Xie, S. Preis, Y. Hu, H. Wu, C. Wei, RSC Advances metal ions and organic acids, (2018) 8950–8960. https://doi.org/10.1039/c7ra11811b.

[61] H. Irving and, R. J. P.Williams, The stability of transition-metal complexes, J. Chem. Soc. (1953) 3192–3210. https://doi.org/10.1039/JR9530003192.